Saudi Pharmaceutical Journal 27 (2019) 303–311

Contents lists available at ScienceDirect

Saudi Pharmaceutical Journal

journal homepage: www.sciencedirect.com

Original article

Triazene salts: Design, synthesis, ctDNA interaction, lipophilicity determination, DFT calculation, and antiproliferative activity against human cancer cell lines

Joanna Cytarska [a,*], Artur Anisiewicz [b], Angelika Baranowska-Łączkowska [c], Adam Sikora [d], Joanna Wietrzyk [b], Konrad Misiura [a], Krzysztof Z. Łączkowski [a]

[a] Department of Chemical Technology and Pharmaceuticals, Faculty of Pharmacy, Collegium Medicum, Nicolaus Copernicus University, Jurasza 2, 85-089 Bydgoszcz, Poland
[b] Institute of Immunology and Experimental Therapy, Polish Academy of Sciences, Rudolfa Weigla 12, 53-114 Wrocław, Poland
[c] Institute of Physics, Kazimierz Wielki University, Plac Weyssenhoffa 11, 85-072 Bydgoszcz, Poland
[d] Department of Analytical Chemistry, Faculty of Pharmacy, Collegium Medicum, Nicolaus Copernicus University, Jurasza 2, 85-089 Bydgoszcz, Poland

ARTICLE INFO

Article history:
Received 28 March 2018
Accepted 22 November 2018
Available online 22 November 2018

Keywords:
Antiproliferative activity
Triazene
Nuclear Magnetic Resonance
Lipophilicity
DNA

ABSTRACT

Synthesis, characterization and investigation of antiproliferative activity of nine triazene salts against human cancer cells lines (MV-4-11, MCF-7, JURKAT, HT-29, Hep-G2, HeLa, Du-145 and DAUDI), and normal human mammary epithelial cell line (MCF7-10A) is presented. The structures of novel compounds were determined using ^{1}H and ^{13}C NMR, and GC-APCI-MS analyses. Among the derivatives, compound **2c**, **2d**, **2e** and **2f** has very strong activity against biphenotypic B myelomonocytic leukemia MV4-11, with IC_{50} values from 5.42 to 7.69 μg/ml. The cytotoxic activity of compounds **2c**-**2f** against normal human mammary gland epithelial cells MCF-10A is 6–11 times lower than against cancer cell lines. Our results also show that compounds **2c** and **2f** have very strong activity against DAUDI and HT-29 with IC_{50} 4.91 μg/ml and 5.59 μg/ml, respectively. Their lipophilicity was determined using reversed-phase ultra-performance liquid chromatography and correlated with antiproliferative activity. Our UV–Vis spectroscopic results indicate also that triazene salts tends to interact with negatively charged DNA phosphate chain. To support the experiment, theoretical calculations of the ^{1}H NMR shifts were carried out within the Density Functional Theory.

1. Introduction

One of the most aggravating diseases in the present world is cancer. Each year more than ten million people are diagnosed with some type of cancer, and more than half of them can die of it. In many countries, cancer diseases occupy the second place immediately after cardiovascular diseases (Boyle and Levin, 2008). Although public awareness about the treatment and prevention of cancer is still growing, and although new anticancer drugs are still being developed, cancer remains the major health problem in the around the world (Ferlay et al., 2013). Many of the current anticancer drugs have very low selectivity, relatively high side effects, limited bioavailability and oral absorption or rapid metabolism (Zawilska et al., 2013). For this reason, many prodrug groups have been developed that are activated in the cancer cells. Such a group of prodrug alkylating agents are triazenes which are successfully used for the fight against many tumors, such as leukemia, lymphoma, melanoma, and sarcoma (Yahalom et al., 1983; Smith et al., 1990). Some triazenes have also been used as a prodrug candidate for melanocyte-directed enzyme prodrug therapy (MDEPT) (Monteiro et al., 2013).

Approved by the Food and Drug Administration (FDA) for medical use Dacarbazine (**1**) (5-(3,3-dimethyltriazene)imidazol-4-carboxamide, DTIC) and Temozolomide (**2**) (8-carbamoyl-3-methyl-imidazol[5,1-*d*]-1,2,3,5-tetrazin-4(3*H*)-one, TMZ) are the only triazenes used in the treatment of cancer (Meer et al., 1986; O'Reilly et al., 1993). DTIC requires activation by the cytochrome P450, resulting in the production of a very reactive methyldiazonium

* Corresponding author at: Department of Chemical Technology and Pharmaceuticals, Faculty of Pharmacy, Collegium Medicum, Nicolaus Copernicus University, Jurasza 2, 85-089 Bydgoszcz, Poland.
E-mail address: cytar@cm.umk.pl (J. Cytarska).
Peer review under responsibility of King Saud University.

Production and hosting by Elsevier

https://doi.org/10.1016/j.jsps.2018.11.012
1319-0164/

cations that can react with DNA O^6-methylguanine, while Temozolomide does not require enzymatic activation and is hydrolysed to the active form already under physiological conditions (Meer et al., 1986; Friedman et al., 2000). However, many types of cancer cells have a mechanism to repair this type of damage by expressing a protein O^6-alkylguanine DNA alkyltransferase thereby reducing the effectiveness of the drugs used (Happold et al., 2012; Kanugula and Pegg, 2003; Friedman et al., 2000).

These results encouraged us to continue our investigation on the synthesis and molecular properties of anticancer agents with divers mechanism of action (Łączkowski et al., 2014; Cytarska et al. 2015; Łączkowski et al., 2016, 2018). Our research began with the design and synthesis of nine novel triazene salts and evaluation of their antiproliferative activity against human cancer cells lines (biphenotypic B myelomonocytic leukemia MV4-11, human breast carcinoma MCF-7, human leukemic T-cell lymphoblast JURKAT, human colon adenocarcinoma HT-29, human hepatocellular carcinoma Hep-G2, human cervical carcinoma HeLa, human prostate carcinoma Du-145, Burkitt lymphoma DAUDI, and normal human mammary epithelial cell line MCF7-10A using the 3-(4,5-dimethyl thiazol-2-yl)-2,5-diphenyltetrazoliun bromide (MTT) or sulforhodamine B (SRB) assays. Moreover, for a better understanding of the mechanism of action we also performed interaction of triazenes with ctDNA using UV–Visible absorption spectroscopic (Sohrabi et al., 2018; Moosavi-Movahedi et al., 2004; Marouzi et al., 2017; Omidvar et al., 2013; Rashidipour et al., 2016; Bakaeean et al., 2012; Moosavi-Movahedi et al., 2003), as well as their lipophilicity parameter. To support the experiment, theoretical calculations of the ^{1}H NMR shifts were carried out within the Density Functional Theory.

2. Experimental

2.1. Materials and methods

All experiments were carried out under air atmosphere unless stated otherwise. Reagents were generally the best quality commercial-grade products and were used without further purification. ^{1}H NMR (700 and 400 MHz) and ^{13}C NMR (100 MHz) spectra were recorded on a Bruker Avance III multinuclear instrument. MS spectra were recorded on triple quadrupole mass spectrometer detector LCMS-8040 (Shimadzu, Japan). Melting points were determined in open glass capillaries and are uncorrected. Analytical TLC was performed using Macherey-Nagel Polygram Sil G/UV$_{254}$ 0.2 mm plates. Bis(2-chloro-ethyl)amine hydrochloride, and appropriate anilines were commercial materials (Aldrich).

2.1.1. 3-(4-Acetylphenyl)-1-(2-chloroethyl)-4,5-dihydro-1H-1,2,3-triazol-3-ium chloride (2a). Typical procedure

1-(4-Aminophenyl)ethanone (1.50 g, 11.1 mmoles) was added to 6 M HCl (3.7 ml) and the reaction mixture was warmed until disappearance of the starting amine. The solution was cooled to 0 °C and sodium nitrite (0.80 g, 11.7 mmoles) in water (2 ml) was added dropwise during 10 min. Then bis(2-chloroethyl)amine hydrochloride (2.18 g, 12.2 mmoles) was slowly added, and next reaction mixture was alkalized with saturated $NaHCO_3$ and left stirring for 15 min. Solid product was filtered, washed with water and dried. Yield: 2.70 g, 84%; mp 121–124 °C decomp., (dichloromethane/methanol, 80:20, R_f = 0.15). ^{1}H NMR (DMSO d_6, 400 MHz), δ (ppm): 2.64 (s, 3H, CH_3); 4.19 (t, 2H, CH_2, J = 5 Hz); 4.63 (t, 2H, CH_2, J = 5 Hz); 4.73 (t, 2H, CH_2, J = 14 Hz); 4.92 (t, 2H, CH_2, J = 13 Hz); 7.75 (d, 2H, 2CH, J = 9 Hz); 8.17 (d, 2H, 2CH, J = 9 Hz). ^{13}C NMR (DMSO d_6, 100 MHz), δ (ppm): 27.31 (CH_3); 40.64 (CH_2); 52.22 (CH_2); 55.43 (CH_2); 55.36 (CH_2); 118.47 (2C_{Ar}); 130.61 (2C_{Ar}); 136.58 (C); 139.89 (C); 197.43 (CO). GC-APCI-MS (m/z, %): 216 [(M^+-2Cl), 100].

2.1.2. 1-(2-Chloroethyl)-3-phenyl-4,5-dihydro-1H-1,2,3-triazol-3-ium chloride (2b)

Yield: 1.67 g, 62%, (dichloromethane/methanol, 80:20, R_f = 0.20); mp 89–91 °C decomp. ^{1}H NMR (DMSO d_6, 700 MHz), δ (ppm): 4.21 (t, 2H, CH_2, J = 5.5 Hz); 4.62 (t, 2H, CH_2, J = 5 Hz); 4.74 (t, 2H, CH_2, J = 14 Hz); 4.95 (t, 2H, CH_2, J = 13 Hz); 7.52 (t, 1H, CH, J = 7 Hz); 7.63 (m, 2H, 2CH); 7.67 (m, 2H, 2CH). ^{13}C NMR (DMSO d_6, 100 MHz), δ (ppm): 40.78 (CH_2); 52.48 (CH_2); 54.94 (CH_2); 54.66 (CH_2); 118.55 (2C_{Ar}); 129.38 (C); 130.56 (2C_{Ar}); 136.71 (C). GC-APCI-MS (m/z, %): 174 [(M^+-2Cl), 100].

2.1.3. 1-(2-Chloroethyl)-3-p-tolyl-4,5-dihydro-1H-1,2,3-triazol-3-ium chloride (2c)

Yield: 2.40 g, 83%, (dichloromethane/methanol, 95:5, R_f = 0.16); mp 107–108 °C decomp. ^{1}H NMR (DMSO d_6, 700 MHz), δ (ppm): 2.40 (s, 3H, CH_3); 4.18 (t, 2H, CH_2, J = 5.5 Hz); 4.57 (t, 2H, CH_2, J = 6 Hz); 4.67 (t, 2H, CH_2, J = 14 Hz); 4.91 (t, 2H, CH_2, J = 12 Hz); 7.44 (d, 2H, 2CH, J = 8 Hz); 7.56 (d, 2H, 2CH, J = 8 Hz). ^{13}C NMR (DMSO d_6, 100 MHz), δ (ppm): 21.08 (CH_3); 40.83 (CH_2); 52.66 (CH_2); 54.37 (CH_2); 54.79 (CH_2); 118.51 (2C_{Ar}); 130.96 (2C_{Ar}); 134.30 (C); 139.43 (C). GC-APCI-MS (m/z, %): 188 [(M^+-2Cl), 100].

2.1.4. 1-(2-Chloroethyl)-3-(3-(trifluoromethyl)phenyl)-4,5-dihydro-1H-1,2,3-triazol-3-ium chloride (2d)

Yield: 1.30 g, 37%, (dichloromethane/methanol, 95:5, R_f = 0.18); mp 131–133 °C decomp. ^{1}H NMR (DMSO d_6, 400 MHz), δ (ppm): 4.20 (t, 2H, CH_2, J = 5 Hz); 4.63 (t, 2H, CH_2, J = 5.5 Hz); 4.75 (t, 2H, CH_2, J = 14 Hz); 4.95 (t, 2H, CH_2, J = 13 Hz); 7.88 (m, 2H, 2CH); 7.96 (m, 2H, 2CH). ^{13}C NMR (DMSO d_6, 100 MHz), δ (ppm): 40.67 (CH_2); 52.46 (CH_2); 55.51 (CH_2); 55.27 (CH_2); 115.37 (q, C, J_{C-F} = 4 Hz); 120.70 (C); 125.60 (q, C, J_{C-F} = 4 Hz); 131.06 (q, C, J_{C-F} = 33 Hz); 131.98 (2C); 137.49 (C). GC-APCI-MS (m/z, %): 242 [(M^+-2Cl), 100].

2.1.5. 1-(2-Chloroethyl)-3-(4-chlorophenyl)-4,5-dihydro-1H-1,2,3-triazol-3-ium chloride (2e)

Yield: 1.44 g, 46%, (dichloromethane/methanol, 80:20, R_f = 0.19); mp 151–156 °C decomp. ^{1}H NMR (DMSO d_6, 400 MHz), δ (ppm): 4.17 (t, 2H, CH_2, J = 5 Hz); 4.58 (t, 2H, CH_2, J = 5.5 Hz); 4.68 (t, 2H, CH_2, J = 14 Hz); 4.88 (t, 2H, CH_2, J = 13 Hz); 7.67 (m, 2H, 2CH); 7.71 (m, 2H, 2CH). ^{13}C NMR (DMSO d_6, 100 MHz), δ (ppm): 40.73 (CH_2); 52.59 (CH_2); 55.13 (2CH_2); 120.40 (2C_{Ar}); 130.48 (2C_{Ar}); 133.50 (C); 135.64 (C). GC-APCI-MS (m/z, %): 208 [(M^+-2Cl), 100].

2.1.6. 1-(2-Chloroethyl)-3-(4-(ethoxycarbonyl)phenyl)-4,5-dihydro-1H-1,2,3-triazol-3-ium chloride (2f)

Yield: 2.80 g, 80%, (dichloromethane/methanol, 80:20, R_f = 0.13); mp 153–154 °C decomp. ^{1}H NMR (DMSO d_6, 700 MHz), δ (ppm): 1.37 (t, 3H, CH_3, J = 7 Hz); 4.21 (t, 2H, CH_2, J = 5 Hz); 4.38 (t, 2H, CH_2, J = 5 Hz); 4.65 (t, 2H, CH_2, J = 13 Hz); 4.75 (t, 2H, CH_2, J = 14 Hz); 4.93 (q, 2H, CH_2, J = 8 Hz); 7.78 (d, 2H, 2CH, J = 9 Hz); 8.18 (d, 2H, 2CH, J = 9 Hz). ^{13}C NMR (DMSO d_6, 100 MHz), δ (ppm): 14.60 (CH_3); 40.64 (CH_2); 52.21 (CH_2); 55.38 (CH_2); 55.49 (CH_2); 61.69 (CH_2); 118.57 (2C_{Ar}); 129.89 (C); 130.47 (2C_{Ar}); 140.07 (C); 165.07 (CO). GC-APCI-MS (m/z, %): 246 [(M^+-2Cl), 100].

2.1.7. 1-(2-Chloroethyl)-3-(4-nitrophenyl)-4,5-dihydro-1H-1,2,3-triazol-3-ium chloride (2g)

Yield: 2.90 g, 91%, (dichloromethane/methanol, 95:5, R_f = 0.12); mp 116–117 °C decomp. ^{1}H NMR (DMSO d_6, 700 MHz), δ (ppm): 4.24 (t, 2H, CH_2, J = 5.5 Hz); 4.71 (t, 2H, CH_2, J = 5 Hz); 4.83 (t, 2H,

CH_2, J = 13 Hz); 4.96 (t, 2H, CH_2, J = 13 Hz); 7.89 (d, 2H, 2CH, J = 9 Hz); 8.48 (d, 2H, 2CH, J = 9 Hz). ^{13}C NMR (DMSO d_6, 100 MHz), δ (ppm): 40.57 (CH_2); 52.15 (CH_2); 55.68 (CH_2); 56.13 (CH_2); 119.30 ($2C_{Ar}$); 126.14 ($2C_{Ar}$); 141.37 (C); 146.81 (C). GC-APCI-MS (*m*/*z*, %): 219 [(M^+-2Cl), 100].

2.1.8. 1-(2-Chloroethyl)-3-(4-(sodiumsulfonate)phenyl)-4,5-dihydro-1H-1,2,3-triazol-3-ium chloride (2h)

Yield: 2.00 g, 52%, (dichloromethane/methanol, 80:20, R_f = 0.10); mp 251–253 °C decomp. ^{1}H NMR (DMSO d_6, 700 MHz), δ (ppm): 4.17 (t, 2H, CH_2, J = 6 Hz); 4.58 (t, 2H, CH_2, J = 5.5 Hz); 4.65 (t, 2H, CH_2, J = 14 Hz); 4.88 (t, 2H, CH_2, J = 15 Hz); 7.58 (d, 2H, 2CH, J = 9 Hz); 7.89 (d, 2H, 2CH, J = 9 Hz). ^{13}C NMR (DMSO d_6), δ (ppm): 40.66 (CH_2); 52.31 (CH_2); 54.78 (CH_2); 54.97 (CH_2); 117.84 ($2C_{Ar}$); 127.59 ($2C_{Ar}$); 136.43 (C); 148.59 (C). GC-APCI-MS (*m*/*z*, %): 276 [(M^+-2Cl), 100].

2.1.9. 1-(2-Chloroethyl)-3-(4-fluorophenyl)-4,5-dihydro-1H-1,2,3-triazol-3-ium chloride (2i)

Yield: 1.30 g, 44%, (dichloromethane/methanol, 80:20, R_f = 0.11); mp 91–93 °C decomp. ^{1}H NMR (DMSO d_6, 400 MHz), δ (ppm): 4.16 (t, 2H, CH_2, J = 6 Hz); 4.56 (t, 2H, CH_2, J = 5.5 Hz); 4.67 (t, 2H, CH_2, J = 13 Hz); 4.90 (t, 2H, CH_2, J = 14 Hz); 7.50 (m, 2H, 2CH); 7.71 (m, 2H, 2CH). ^{13}C NMR (DMSO d_6, 100 MHz), δ (ppm): 40.78 (CH_2); 52.88 (CH_2); 54.82 (CH_2); 54.92 (CH_2); 117.52 (d, $2C_{Ar}$, J_{C-F} = 24 Hz); 121.27 (d, $2C_{Ar}$, J_{C-F} = 9 Hz); 133.30 (d, C, J_{C-F} = 2 Hz); 160.80 (C). GC-APCI-MS (*m*/*z*, %): 192 [(M^+-2Cl), 100].

2.2. Biological activity

2.2.1. Cells

Human cancer cell lines Du-145, HeLa, HepG2, HT-29, MCF-7, MV-4-11 and normal human mammary gland epithelial cells MCF-10A were obtained from American Type Culture Collection (Rockville, Maryland, USA). DAUDI and Jurkat cell lines were purchased from Leibniz Institute DSMZ-German Collection of Microorganisms and Cell Cultures. All cell lines were maintained in liquid nitrogen at the Cell Culture Collection of Institute of Immunology and Experimental Therapy (Wroclaw, Poland). The Du-145 and MCF-7 cell lines were grown in Eagle's medium (IIET, Wroclaw, Poland) with addition of 10% fetal bovine serum (Sigma-Aldrich, Steinheim, Germany). Medium of MCF-7 was supplemented with MEM Non-Essential Amino Acids Solution, 2.0 mM L-glutamine and 8 μg/ml of insulin (all Sigma-Aldrich, Steinheim, Germany) and medium of DU-145 was enriched by 1.0 mM sodium pyruvate and 4.0 mM L-glutamine (both Sigma-Aldrich, Steinheim, Germany). The HeLa and HT-29 cell lines were maintained in a mixture of RPMI + HEPES medium and Opti-MEM medium (1:1, IIET, Wroclaw, Poland) with the addition of 5% fetal bovine serum (HyClone, GE Healthcare, UK), 2.0 mM L-glutamine and 1.0 mM sodium pyruvate (both Sigma-Aldrich, Steinheim, Germany). HepG2 cells was cultured in Dulbecco medium DMEM (Gibco, Scotland, UK) with 10% fetal bovine serum (HyClone, GE Healthcare, UK) and 2.0 mM L-glutamine (Sigma-Aldrich, Steinheim, Germany). DAUDI, Jurkat and MV-4-11 cell lines were grown in RPMI 1640 medium with GlutaMAX (Gibco, Scotland, UK) with addition of 10% fetal bovine serum (Sigma-Aldrich, Steinheim, Germany). The medium of MV-4-11 cells was supplemented in 1 mM sodium pyruvate (Sigma-Aldrich, Germany). MCF-10A cells were maintained in Ham's F-12 Nutrient Mixture with 5% horse serum (both Gibco, Scotland, UK). The MCF10A medium was enriched by 10 μg/ml of insulin, 0.5 μg/ml of hydrocortisone, 0.05 μg/ml of cholera toxin from *Vibrio Cholerae* and 20 ng/ml of human epidermal growth factor (all Sigma-Aldrich, Steinheim, Germany). All culture media were supplemented with 100 units/mL penicillin (Polfa Tarchomin S.A., Warsaw, Poland) and 100 μg/mL streptomycin (Sigma-Aldrich, Steinheim, Germany). The cell lines were cultured at 37 °C in a humid atmosphere saturated with 5% CO_2.

2.2.2. Compounds

Prior to usage, the compounds were dissolved in DMSO and culture medium (1:9) to the concentration of 1 mg/ml, and subsequently diluted in culture medium to reach the required concentrations (0.1, 1, 10 and 100 μg/ml).

2.2.3. In vitro antiproliferative assay

The cells were plated in 96-well plates (Sarstedt, Germany) in an appropriate density: 1×10^4 per well for DAUDI, Du-145, Jurkat, Hep-G2, MV-4-11 and MCF-10A, 0.75×10^4 per well for HT-29 and MCF-7 and 0.25×10^4 per well for HeLa cell line. After twenty four hours the cultured cell lines were exposed to different concentrations of the tested agents for 72 h (total plate incubation time: 96 h). To determine cytotoxicity of tested agents, the antiproliferative tests were performed as previously described (Wietrzyk et al., 2007). The MTT assay was performed for DAUDI, Jurkat, MV-4-11 and the SRB assay was conducted for DU-145, HeLa, HepG-2, HT-29, MCF-7, MCF-10A cell lines. The results were presented as an IC_{50} values (inhibitory concentration 50) – the dose (μg/mL) of tested compounds that inhibits cell proliferation at 50%. Each concentration of examined agents was tested in triplicate in a single experiment, which was repeated at least 3 times (Rubinstein et al., 1990; Bramson et al., 1995). The activity of examined agents was compared to the activity of reference compound – *cis*-platin (Accord Healthcare Polska, Warsaw, Poland). The control of 99.8% ethanol that was the solvent of the tested agents was also performed.

2.2.4. SRB cytotoxic test

Cells were attached to the bottom of plastic wells by fixing them with cold 50% TCA (trichloroacetic acid, POCH, Gliwice, Poland) on top of the culture medium in each well. The plates were incubated at 4 °C for 1 h and then washed five times with tap water. The cellular material fixed with TCA was stained with 0.14% sulforhodamine B (SRB, Sigma-Aldrich, Germany) and dissolved in 1% acetic acid (POCH, Gliwice, Poland) for 30 min. Unbound dye was removed by rinsing (4X) in 1% acetic acid. The protein-bound dye was extracted with 10 mM unbuffered Tris base (Sigma-Aldrich Chemie GmbH, Steinheim, Germany) for determination of the optical density (λ = 540 nm) in a computer-interfaced, 96-well Synergy H4 (BioTek Instruments USA) photometer microtiter plate reader (Sidoryk et al., 2012).

2.2.5. MTT cytotoxic test

20 μl of MTT solution (MTT: 3-(4,5-dimethylthiazol-2-yl)-2,5-diphenyl tetrazolium bromide, stock solution: 5 mg/ml) was added to each well and incubated for 4 h. After the incubation time was complete, 80 μl of the lysis mixture was added to each well (lysis mixture: 225 ml dimethylformamide, 67.5 g sodium dodecyl sulfate and 275 ml of distilled water). The optical densities of the samples were read after 24 h on a Synergy H4 (BioTek Instruments USA) photometer microtiter plate reader at 570 nm (Sidoryk et al., 2012). All of chemicals were obtained from Sigma-Aldrich, Germany.

2.3. Determiantion of lipophilicity by RP UPLC

The studies were performed on the UPLC–MS/MS system equipped with solvent delivery two pumps LC-30AD combined with gradient systems, degasser model DGU-20A5, an autosampler model SIL-30AC, a column oven model CTO-20AC, UV detector model SPD-M20A and triple quadrupole mass spectrometer

detector LCMS-8040 (Shimadzu, Japan). Kinetex C18 (150 × 4.6 mm; 2.6 μm) column was purchased from Phenomenex Co. The methanol concentration, expressed in volumetric ratio v/v, ranged from 0.65 to 0.95 in constant steps of 0.05. Tested compounds were dissolved in methanol (10 μg/ml). The flow rate of the mobile phase was 0.5 ml/min. All analyses were carried out at 25 °C, and detection wavelength of 254 nm was chosen.

2.4. Spectroscopy

The UV absorption spectra were recorded on T60U spectrophotometer (PG Instruments) equipped with quartz cells of 1 cm path length; the pH value of the solutions were determined with CP-501 pH-meter (Elmetron). ctDNA, ethidium bromide dye (EB) and Tris were obtained from the Sigma-Aldrich Company. Tris-HCl buffer solution (concentration 10 mM) was prepared by dissolving solid substance in doubly distilled water and acidify by HCl to pH 7.4. The stock solution of ctDNA was prepared by dissolving solid substance in Tris-HCl buffer. EB solution was prepared by dissolving solid substance in ethanol and Tris-HCl solution. All solutions were stored at 4 °C. The concentrations of ctDNA and EB were determined by absorption spectroscopy using the molar extinction coefficient of 6600 M^{-1} cm^{-1} at 260 nm and 5800 M^{-1} cm^{-1} at 480 nm, respectively. The solutions of ctDNA had a ratio of UV absorbance at 260 and 280 nm larger than 1.8, which indicated that ctDNA was sufficiently free from protein. The stock solutions of substances of **2a-2i** series at concentration 100 mM were prepared by dissolving solid substance in ethanol and Tris-HCl solution (1:10) (Charak et al., 2012).

2.5. Quantum mechanical calculations

Theoretical evaluation of NMR proton chemical shifts was carried out for all investigated compounds employing Density Functional Theory (DFT) approximation. As a first step, optimization of investigated systems geometrical parameters was carried out at the B3LYP/6-311G** level of theory and followed by frequency calculations to confirm that the resulting structures correspond to real minima on the potential energy surface. Single starting point per system was used. Next, chemical shifts were calculated with respect to tetramethylsilane (TMS) and compared to experimental data recorded in DMSO. Based on results of our earlier theoretical study of NMR shifts in similar compounds (Baranowska-Łączkowska et al., 2018) we used M06 and B3LYP functionals, combining them with the aug-pcS-1 basis set of Jensen (Jensen, 2008). London Atomic Orbitals (LAOs) (London, 1937) were employed to ensure gauge-origin independent results. Solvent effects were not included in the calculations, as the proton shifts of investigated compounds are not expected to be strongly solvent-dependent. All calculations were carried out using the Gaussian 09 package (Frisch et al., 2009). The aug-pcS-1 basis set was taken from the EMSL Basis Set Library (Feller, 1996; Schuchardt et al. 2007).

3. Results and discussion

3.1. Chemistry

The target triazene salts containing chloroethyl group were obtained in two steps, one-flask synthesis. In the first step, *para*- or *meta*-substituted benzenediazonium chlorides were prepared by diazotization reaction of appropriate anilines **1a-1i** in the presence of sodium nitrite in 6 M hydrochloric acid (Scheme 1). In the next step, a series of triazene **2a-2i** was synthesized by reaction between different substituted benzenediazonium chlorides and bis(2-chloroethyl)amine hydrochloride, followed by addition of sodium hydrogen carbonate, with good yield (37–91%) and chemical purity. All of the synthesized derivatives were characterized by spectroscopic methods ^{1}H NMR (700 MHz) and ^{13}C NMR (100 MHz), and GC-APCI-MS analyses. ^{1}H NMR and ^{13}C NMR spectra of triazenes **2a-2i** showed four characteristic triplets at δ (4.16–4.96 ppm) and peaks at δ (40.57–56.13 ppm) due to the four methylene groups, which indicates the conversion of substrates to the expected products with the simultaneous creation of internal triazene salts **2a-2i**. The mass spectra of all compounds showed (M+-2Cl) ion in the positive-ion mode which is fully consistent with the assigned structures.

3.2. Calculations

To further confirm the structure of resulting triazene salts **2a-2i**, theoretical evaluation of NMR proton chemical shifts was carried out for all investigated compounds employing Density Functional Theory (DFT) approximation. Resulting theoretical chemical shifts are presented in (Table 1) together with the corresponding experimental data. Values of the root mean square error (rmse) calculated with respect to experimental data are also printed. Complete set of geometrical parameters of investigated systems can be found in Supplementary Material. We note here that all calculations have been carried out employing frozen structures, and thus protons being chemically equivalent due to rotations around single bonds, and leading to single experimental signal, in our calculations have different chemical environment and appear at different chemical shifts.

For the purpose of comparison with experimental data average theoretical chemical shifts are thus calculated from chemical shifts of protons which would be chemically equivalent. Next

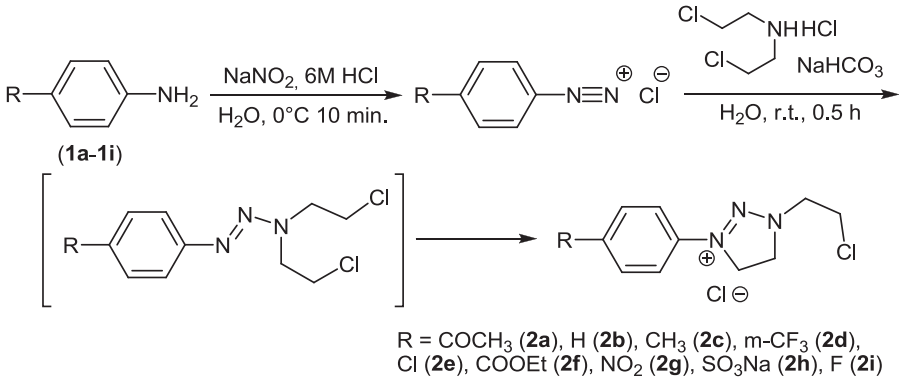

Scheme 1. Synthesis of triazene salts **2a-2i**.

Table 1
DFT chemical shifts (ppm) of compounds **2a-2i**, together with the experimental values recorded in DMSO.

Triazene **2a-2i**																		RMSE
2a	H_{18}	H_{19}	H_{20}	H_{21}	H_{22}	H_{23}	H_{24}	H_{25}	H_{26}	H_{29}	H_{27}	H_{28}	H_{30}	H_{31}	H_{32}			
δ_{B3LYP}	4.50	4.33	4.77	4.76	3.91	4.64	3.68	3.80	8.10	7.08	8.28	8.93	2.79	2.79	2.69			0.31
δ_{M06}	4.54	4.34	4.83	4.76	3.98	4.67	3.58	3.81	8.17	7.21	8.37	9.08	2.79	2.75	2.68			0.33
δ_{exp}	4.73		4.92		4.63		4.19		7.75		8.17		2.64					
2b	H_{15}	H_{16}	H_{17}	H_{18}	H_{19}	H_{20}	H_{21}	H_{22}	H_{23}	H_{27}	H_{24}	H_{26}	H_{25}					
δ_{B3LYP}	4.48	4.31	4.74	4.77	3.88	4.61	3.69	3.78	8.05	7.06	7.91	7.86	7.91					0.32
δ_{M06}	4.51	4.34	4.74	4.75	3.92	4.58	3.65	3.78	8.10	7.12	7.92	7.91	8.01					0.34
δ_{exp}	4.74		4.95		4.62		4.21		7.63		7.67		7.52					
2c	H_{20}	H_{21}	H_{22}	H_{23}	H_{24}	H_{25}	H_{26}	H_{27}	H_{16}	H_{17}	H_{18}	H_{19}	H_{28}	H_{29}	H_{30}	.	.	
δ_{B3LYP}	4.44	4.27	4.71	4.73	3.83	4.57	3.66	3.76	6.87	7.91	7.71	7.62	2.77	2.77	2.36			0.28
δ_{M06}	4.45	4.28	4.71	4.73	3.89	4.57	3.61	3.76	6.96	8.02	7.73	7.64	2.73	2.71	2.32			0.28
δ_{exp}	4.67		4.91		4.57		4.18		7.44		7.56		2.40					
2d	H_{19}	H_{20}	H_{21}	H_{22}	H_{23}	H_{24}	H_{25}	H_{26}	H_{27}	H_{28}	H_{29}	H_{30}						
δ_{B3LYP}	4.55	4.37	4.75	4.74	3.94	4.66	3.69	3.79	8.50	8.26	7.98	7.13						
δ_{M06}	4.58	4.37	4.81	4.72	3.96	4.72	3.59	3.76	8.56	8.36	8.08	7.26						
δ_{exp}	4.75		4.95		4.63		4.20		7.88, 7.96									
2e	H_{16}	H_{17}	H_{18}	H_{19}	H_{20}	H_{21}	H_{22}	H_{23}	H_{24}	H_{27}	H_{25}	H_{26}						
δ_{B3LYP}	4.47	4.31	4.70	4.70	3.87	4.59	3.67	3.77	7.88	6.88	7.82	7.77						0.30
δ_{M06}	4.49	4.31	4.72	4.68	3.93	4.60	3.59	3.77	7.96	6.97	7.85	7.81						0.29
δ_{exp}	4.68		4.88		4.58		4.17		7.67		7.71							
2f	H_{20}	H_{21}	H_{22}	H_{23}	H_{24}	H_{25}	H_{26}	H_{27}	H_{28}	H_{31}	H_{29}	H_{30}	H_{32}	H_{33}	H_{34}	H_{35}	H_{36}	
δ_{B3LYP}	4.50	4.32	4.73	4.79	3.90	4.62	3.67	3.80	7.95	7.09	7.94	8.44	1.20	1.84	1.51	4.01	4.49	0.28
δ_{M06}	4.48	4.28	4.77	4.79	3.98	4.68	3.63	3.80	7.97	7.24	8.12	8.57	1.09	1.81	1.45	3.98	4.41	0.28
δ_{exp}	4.75		4.93		4.65		4.21		7.78		8.18		1.37			4.38		
2g	H_{18}	H_{19}	H_{20}	H_{21}	H_{22}	H_{23}	H_{24}	H_{25}	H_{26}	H_{29}	H_{27}	H_{28}						
δ_{B3LYP}	4.58	4.40	4.77	4.74	3.97	4.68	3.70	3.82	8.07	7.07	8.97	8.96						0.38
δ_{M06}	4.61	4.41	4.81	4.73	4.04	4.71	3.60	3.82	8.13	7.16	9.05	9.11						0.40
δ_{exp}	4.83		4.96		4.71		4.24		7.89		8.48							
2h	H_{20}	H_{21}	H_{22}	H_{23}	H_{24}	H_{25}	H_{26}	H_{27}	H_{28}	H_{31}	H_{29}	H_{30}						
δ_{B3LYP}	4.43	4.29	4.69	4.77	3.85	4.60	3.67	3.77	7.90	6.93	8.44	8.39						0.35
δ_{M06}	4.45	4.25	4.77	4.76	3.87	4.63	3.64	3.81	7.95	7.04	8.58	8.54						0.38
δ_{exp}	4.65		4.88		4.58		4.17		7.58		7.89							
2i	H_{16}	H_{17}	H_{18}	H_{19}	H_{20}	H_{21}	H_{22}	H_{23}	H_{24}	H_{27}	H_{25}	H_{26}						
δ_{B3LYP}	4.48	4.31	4.70	4.73	3.87	4.59	3.67	3.77	7.99	7.00	7.56	7.49						0.27
δ_{M06}	4.51	4.33	4.70	4.72	3.94	4.59	3.61	3.77	8.09	7.10	7.57	7.54						0.27
δ_{exp}	4.67		4.90		4.56		4.16		7.50[a]		7.71[a]							

[a] Opposite assignment is made based on the M06/aug-pc-1 results. See text for details.

experimental signals are assigned to the respective protons based on the comparison of theoretical and experimental values.

The assignments made based on the B3LYP results agree very well with those made on the M06 values, with the former functional leading in general to slightly smaller rmse values. An exception is observed in the case of molecule **2i**, for which the two functionals yield opposite assignments of aromatic protons signals. Precisely, the B3LYP calculation allows to assign signal of 7.50 ppm to protons H_{24} and H_{27}, and 7.71 ppm to protons H_{25} and H_{26}, while opposite conclusion is made based on the M06 results. Both, theoretical and experimental spectra of all investigated systems confirm assumed structure of the products, and thus mechanism of reaction. Detailed analysis reveals that signals corresponding to protons of 2-chloroethyl group and 1,2,3-triazene ring appear in all investigated systems at approximately constant ppm values, maximum differences being in the order of 0.05–0.20 ppm. This is in line with our expectations, as all these protons are relatively far from the changing substituent whose influence is thus very small. In contrary, the signals of aromatic protons are much more sensitive to the change of the nearby substituent, and their position changes up to 0.9 ppm.

3.3. Lipophilicity determination

The ability to penetrate the drug through biological membranes is the decisive parameter responsible for its activity. Parameter describing this property is lipophilicity that is defined as the partition coefficient between the an aqueous phase and the non-aqueous phase usually 1-octanol and is expressed as log P (Arnott et al., 2012). One of the best methods to determine concentration of a compound in various solvents needed to determine lipophilicity is reversed-phase high performance liquid chromatography (RP-HPLC) (Marciniec et al., 2016). Therefore, for the determination of relative lipophilicity of triazene derivatives **2a-2i** we used reversed-phase ultra-performance liquid chromatography (RP UPLC), based upon sub 3-μm porous particles. Chromatographic capacity factors (k) were calculated: $k = (t_R/t_M) - 1$, where t_R [min] denotes retention time, and t_M [min] is time for dead volume. The dead time was determined using uracil as a t_M marker. Linear relationship between the log k and the concentration of the organic modifier in the mobile phase (methanol) was determined on the basis of the Soczewiński-Wachtmeister equation: $\log k = \log k_w + S\Phi$, where $\log k_w$ denotes the capacity factor of the analyte in pure water, Φ is organic modifier concentration in the mobile phase, and S denotes slope of the regression curve. The lipophilicity parameter Φ_0 was calculated using relationship $\Phi_0 = -\log k_w/S$, and R^2 is correlation coefficient. Experimentally determined lipophilic parameters $\log k_w$ are presented in (Table 2).

In our research we have observed the linear dependence between log k values and concentration of organic modifier in the eluent with correlation coefficient ($R^2 = 0.967–0.998$) value. The analysis shows that the value of the $\log k_w$ is in the range from −3.503 to −0.914. From all tested compounds, the lowest $\log k_w$ values, in the range from −3.503 to −2.675, were observed for compound **2c**, **2d**, **2e** and **2f** containing methyl, trifluoromethyl, chloride and carboxyethyl substituents respectively. The compounds **2a**, **2b**, **2g**, and **2i** containing acetyl, hydrogen, nitro, and fluoro substituents, showed average values of $\log k_w$, in the range from −2.002 to −1.478. The highest value of the $\log k_w$ was found for compounds **2h** containing sodium sulfonate group ($\log k_w$

Table 2
The lipophilicity parameters determined by RP UPLC-MS/MS analysis.

	2a	2b	2c	2d	2e	2f	2g	2h	2i
log k_w	−1.478	−2.002	−2.675	−3.373	−3.503	−2.938	−1.504	−0.914	−1.873
-S	0.755	1.318	2.000	2.802	2.928	2.259	0.594	0.709	1.027
Φ_0	1.958	1.519	1.338	1.204	1.196	1.301	2.532	1.289	1.824
R^2	0.969	0.985	0.998	0.990	0.984	0.993	0.967	0.980	0.971

−0.914). Also, log k_w of the derived compounds increases in the series of substituents: F (**2e**) < Cl (**2i**), and CH_3 (**2c**) < $COCH_3$ (**2a**).

3.4. Biological evaluation

All the synthesized compounds were investigated *in vitro* for their antiproliferative activity against eight human cancer cell lines (MV-4-11, MCF-7, JURKAT, HT-29, Hep-G2, HeLa, Du-145 and DAUDI) and normal human mammary gland epithelial cells MCF-10A using *cis*-platin as positive control and are summarized in (Table 3).

According to our results, compounds **2c, 2d, 2e** and **2f** have very strong activity against biphenotypic B myelomonocytic leukemia MV4-11, with IC_{50} values from 5.42 to 7.69 μg/ml, while their cytotoxic activity against normal human mammary gland epithelial cells MCF-10A is 6–11 times lower. Compound **2c** showed also very strong activity against Burkitt lymphoma DAUDI while compound **2f** showed very strong activity against human colon adenocarcinoma HT-29, with IC_{50} 4.91 μg/ml and 5.59 μg/ml, respectively. Cytotoxic activity of compounds **2c** and **2f** against normal human MCF-10A cells is 8–13 times lower than against these cancer cell lines. Also, our data showed that compound **2a** and **2g** has good activity against MV4-11 cell line, with IC_{50} 13.42 μg/ml and 14.05 μg/ml, respectively.

Compounds **2c**, **2d**, and **2e** also show good activity in relation to other cell lines, MCF-7, JURKAT, HT-29, Hep-G2, HeLa, Du-145 and DAUDI with IC_{50} values from 12.53 to 36.44 μg/ml, and the cytotoxic activity of these compounds against normal human MCF-10A cells is 1–5 times lower than against cancer cell lines.

The structure-activity relationship (SAR) study revealed that triazene derivatives **2c, 2d,** and **2e** containing methyl, trifluoromethyl and chloro substituents showed the highest antiproliferative activity against all reference cancer cell lines. Also compound **2f,** obtained from benzocaine – commonly used anesthetic, and containing carboxyethyl group, showed very high activity against some cancer cell lines. The most active compounds **2c**, **2d**, **2e** and **2f** simultaneously have the lowest lipophilicity, with the log k_w values in the range from −3.503 to −2.675. Compound **2h** containing the -SO_3Na moiety did not show activity over any cancer line investigated, and is characterized by the highest lipophilicity (log k_w −0.914) of all tested compounds. The highest lipophilicity of triazene salt **2h** relative to other derivatives can be explained by the probable formation of zwitterion containing a positive quaternary ammonium cation and negative sulfonate anion. Additional forces in such salts probably play a significant role in the final lipophilicity profile of this compound, however, this problem requires further investigation (Mazák et al., 2011).

3.5. Spectroscopic properties

One of the most important targets of anti-cancer drugs is DNA, so understanding the mechanism of interaction with DNA provides further insight into the possible path of gene expression. Currently, the three main mechanisms of interaction of drugs with DNA are electrostatic interaction between the cationic species and the negatively charged DNA phosphate chain, which is on the outside of the helix, intercalation with the base pairs, and groove binding involving van der Waals bonds (Zhang et al., 2011; Rafique et al., 2013). In order to understand the mechanism of action of the triazenes **2a**-**2i**, their interactions with calf-thymus DNA using UV–Vis spectroscopy were investigated. Calf-thymus DNA is currently the most commonly used DNA, which is derived from calf thymus tissue. It contains 41.9% G-C and 58.1% A-T base pairs. The UV–Vis absorbance spectra of pure triazenes exhibit two absorption bands in the 330–340 (nm) and 221–260 (nm) ranges (Table 4).

Table 4
UV–Vis spectra of triazenes **2a**-**2i**.

Triazene salts	λ_1 (nm)	λ_2 (nm)
2a	335	240
2b	331	236
2c	340	241
2d	326	234
2e	337	223
2f	333	235
2g	340	221
2h	330	–
2i	332	237

Table 3
Antiproliferative activity of triazene nitrogen mustards **2a-2i** against cancer cell lines and normal human mammary epithelial cells MCF-10A.

	IC_{50} ± SD [μg/ml]								
Triazene	MV-4-11	MCF-7	JURKAT	HT-29	Hep-G2	HeLa	Du-145	DAUDI	MCF-10A
2a	13.42 ± 5.937	45.07 ± 1.654	66.20 ± 13.428	49.32 ± 17.381	38.45 ± 12.341	39.42 ± 9.768	88.95 ± 9.309	16.07[a] ± 26.485	79.98 ± 8.431
2b	44.59 ± 4.369	50.44 ± 8.079	68.54 ± 6.356	48.88 ± 18.718	37.93 ± 17.106	39.41 ± 11.465	38.58[a] ± 8.824	40.19 ± 4.286	29.83[a] ± 13.201
2c	5.42 ± 2.523	19.75 ± 3.017	13.14 ± 0.503	16.25 ± 7.374	23.81 ± 5.363	18.11 ± 7.036	36.44 ± 5.287	4.91 ± 1.527	61.64 ± 13.066
2d	5.59 ± 3.033	16.47 ± 4.144	24.29 ± 1.221	31.74 ± 5.453	14.92 ± 1.079	22.70 ± 2.975	30.95 ± 3.146	17.63 ± 2.288	32.62 ± 2.787
2e	7.69 ± 3.169	15.09 ± 2.773	13.64 ± 3.002	31.94 ± 8.143	14.91 ± 4.658	12.53 ± 2.234	30.10 ± 10.156	13.64 ± 3.656	49.34 ± 15.485
2f	6.16 ± 1.763	20.87 ± 2.194	35.98 ± 7.111	5.59 ± 0.632	27.79 ± 10.104	23.51 ± 3.316	22.78 ± 10.062	61.89 ± 24.810	42.04 ± 17.314
2g	14.05 ± 7.746	23.88 ± 7.482	49.11 ± 14.143	47.64 ± 3.418	32.07 ± 1.399	28.97 ± 5.351	34.14 ± 1.350	−61.13[a] ± 60.483	36.61 ± 9.520
2h	−50.8[a] ± 36.576	−5.5[a] ± 14.192	−7.92[a] ± 11.711	−13.65[a] ± 12.306	−27.2[a] ± 17.459	−6.65[a] ± 24.065	−11.95[a] ± 15.547	−89.97[a] ± 18.485	1.02[a] ± 0.478
2i	51.38 ± 11.917	61.40 ± 21.808	39.53[a] ± 10.080	45.17[a] ± 4.094	70.17 ± 13.874	51.26 ± 14.724	35.09[a] ± 7.588	75.60 ± 17.762	15.66[a] ± 4.010
***cis*-platin**	0.76 ± 0.184	1.73 ± 0.443	0.24 ± 0.056	3.63 ± 0.715	0.68 ± 0.147	0.37 ± 0.137	0.59 ± 0.086	1.07 ± 0.208	4.65 ± 1.171

[a] Average proliferation inhibition at 100 μg/ml.

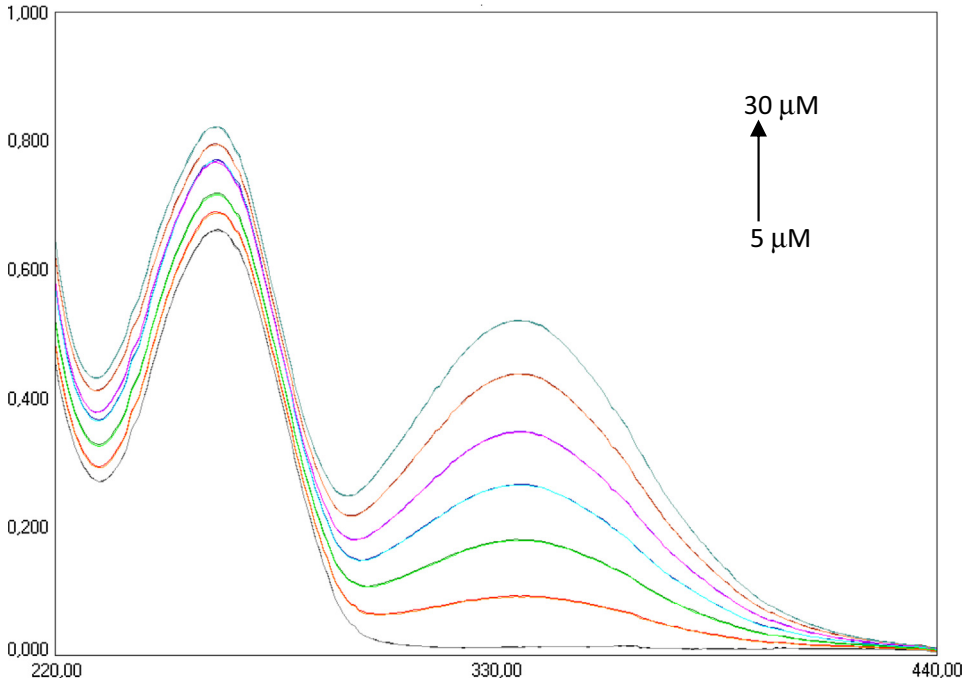

Fig. 1. The absorption spectrum of the solution containing 100 mM of DNA and increasing amounts of **2a**.

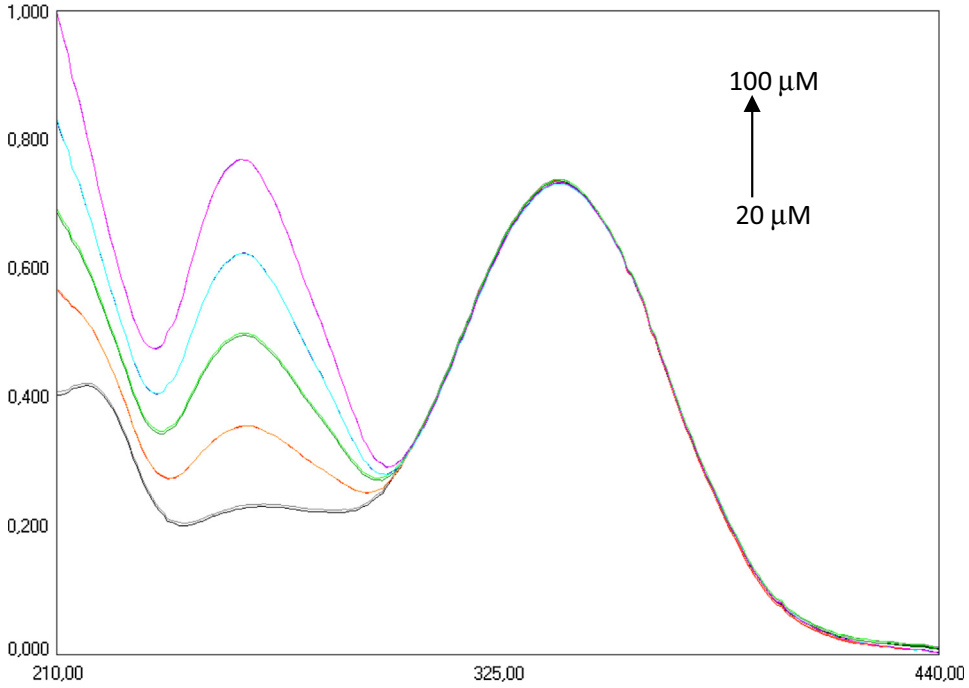

Fig. 2. The absorption spectrum of the solutions containing 30 µM of **2g** and increasing amounts of DNA.

For all compounds with increasing concentration of the triazene with constant DNA concentration, the hyperchromic effect was observed (Fig. 1). The absorption of DNA-triazene complexes at 258 nm showed a decrease in absorbance compared to the sum of the individual components, which clearly shows that the test compounds interact with DNA. With increasing concentration of the DNA at a constant triazene concentration, the hypsochromic shifts were observed relative to the sum of the absorbances of the individual components (Fig. 2). Both in experiments with constant DNA concentration and with a constant concentration of

Table 5
The binding constant K_b between triazenes **2a**-**2i** and DNA.

Triazene	Binding constant K_b [M^{-1}]	Binding constant K_b
2a	55,330	$5.53 \times 10^4\ M^{-1}$
2b	19,758	$1.98 \times 10^4\ M^{-1}$
2c	23,248	$2.32 \times 10^4\ M^{-1}$
2d	19,503	$1.95 \times 10^4\ M^{-1}$
2e	24,968	$2.50 \times 10^4\ M^{-1}$
2f	58,260	$5.83 \times 10^4\ M^{-1}$
2g	26,037	$2.60 \times 10^4\ M^{-1}$
2h	23,427	$2.34 \times 10^4\ M^{-1}$
2i	19,254	$1.92 \times 10^4\ M^{-1}$

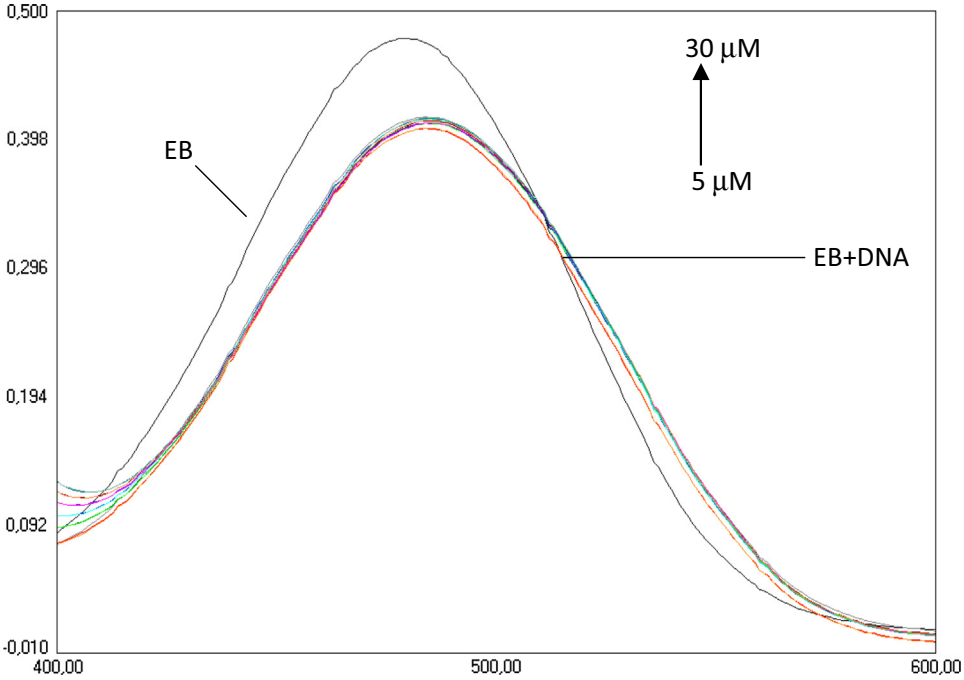

Fig. 3. The absorption spectrum of the solutions containing 80 µM EB, 80 µM DNA and increasing concentration of **2f**.

compounds, the incubation time does not play a key role in the formation of DNA linkage, suggesting a fast bonding to DNA.

In the next step of our research we calculated the intrinsic binding constant K_b between triazene salts **2a**-**2i** and DNA (Table 5) using the equation: $[DNA]/(\varepsilon_a - \varepsilon_f) = [DNA]/(\varepsilon_b - \varepsilon_f) + 1/K_b(\varepsilon_b - \varepsilon_f)$, where [DNA] is the concentration of DNA in base pairs, while ε_a, ε_f and ε_b are the apparent, free and bound complex extinction coefficients, respectively (Pakravan et al., 2015). Plot of $[DNA]/\varepsilon_a - \varepsilon_b \times 10^8$ vs. [DNA] for triazene **2g** can be found in Supplementary Material.

As we can see that the largest binding constant K_b equals $5.83 \times 10^4\ M^{-1}$ (**2f**) and $5.53 \times 10^4\ M^{-1}$ (**2b**) have compounds having the COOEt and $COCH_3$ groups, which is probably caused by the formation of an additional hydrogen bond between the carbonyl group of these compounds and phosphate chain of DNA. The compounds containing NO_2 and Cl groups are characterized by two times smaller binding constant K_b equals $2.60 \times 10^4\ M^{-1}$ and $2.50 \times 10^4\ M^{-1}$, respectively. An interesting observation is also that compounds containing strong electron-withdrawing CF_3 and F groups are characterized by the smallest binding constant $K_b = 1.95 \times 10^4\ M^{-1}$ and $1.92 \times 10^4\ M^{-1}$, respectively. This is probably due to the weakening of the formation of hydrogen bonds by these molecules.

The next experiment with the competitive replacement of ethidium bromide dye (EB) from its complex with DNA by the tested compounds showed no changes in absorbance spectra, suggesting non-intercalative mode of binding between triazenes and DNA (Fig. 3).

In conclusion, our research suggests that cationic triazene species interact fast with the negatively charged DNA phosphate chain outside of the helix.

4. Conclusion

In summary, we have developed an efficient method for the synthesis of triazene salts and confirmed their structure by spectroscopic methods and theoretical calculations. As a result of our research, we have identified new leading structures with very high activity against some types of cancer cells with IC_{50} values from 4.91 to 7.69 µg/ml, and with cytotoxic activity against normal human mammary gland epithelial cells MCF-10A from 6 to 11 times lower than against cancer cell lines. We have also demonstrated a good correlation between determined lipophilicity and the antiproliferative activity of obtained compounds. Our UV–Vis spectroscopic results indicate also that triazene salts tend to interact with negatively charged DNA phosphate chain. Additional calculations show that compounds **2f** and **2b** containing COOEt and $COCH_3$ substituents bind more strongly to DNA than other compounds, their K_b values are $5.83 \times 10^4\ M^{-1}$ and $5.53 \times 10^4\ M^{-1}$, respectively. Moreover, the calculated binding constant K_b values indicates that the resulting derivatives could also interact with DNA in an *in vivo* situation, however, to confirm this further studies are required.

Conflict of interest

The authors confirm that this article content has no conflicts of interest.

Acknowledgements

This study was supported by the Nicolaus Copernicus University (project No. 786/2014).

Appendix A. Supplementary material

Supplementary data to this article can be found online at https://doi.org/10.1016/j.jsps.2018.11.012.

References

Arnott, J.A., Planey, S.L., 2012. The influence of lipophilicity in drug discovery and design. Expert Opin. Drug Discov. 7, 863–875.
Bakaeean, B., Kabiri, M., Iranfar, H., Saberi, M.R., Chamani, J., 2012. Binding effect of common ions to human serum albumin in the presence of norfloxacin:

investigation with spectroscopic and zeta potential approaches. J. Sol. Chem. 41, 1777–1801.
Baranowska-Łączkowska, A., Kozak, M., Łączkowski, K.Z., Fernández, B., 2018. Theoretical calculation of NMR shifts in newly developed antibacterial 4-formylbenzoic acid based thiazoles. Theor. Chem. Acc. 137, 46 (1–10).
Boyle, P., Levin, B., World cancer report 2008. Lyon: International Agency for Research on Cancer; 2008. Reference available from: http://www.iarc.fr/en/publications/pdfs online/wcr/2008/wcr_2008.pdf.
Bramson, J., McQuillan, A., Aubin, R., Alaoui-Jamali, M., Batist, G., Christodoulopoulos, G., Panasci, L.C., 1995. Nitrogen mustard drug resistant B-cell chronic lymphocytic leukemia as an in vivo model for crosslinking agent resistance. Mut. Res. 336, 269–278.
Charak, S., Shandilya, M., Tyagi, G., Mehrotra, R., 2012. Spectroscopic and molecular docking studies on chlorambucil interaction with DNA. Int. J. Biol. Macromolec. 51, 406–411.
Cytarska, J., Skowerski, K., Jaworski, S., Misiura, K., Filip-Psurska, B., Wietrzyk, J., 2015. The disulfide analogues of isophosphoramide mustard for anticancer therapy. Lett. Drug Des. Discov. 12, 172–179.
Feller, D., 1996. The role of databases in support of computational chemistry calculations. J. Comp. Chem. 17, 1571–1586.
Ferlay, J.S.I., Ervik, M., Dikshit, R., Eser, S., Mathers, C., Rebelo, M., Parkin, D.M., Forman, D., Bray, F., 2013. Cancer Incidence and Mortality Worldwide: IARC CancerBase No. 11 [Internet]; GLOBOCAN 2012 v1.0 2013; International Agency for Research on Cancer: Lyon, France.
Friedman, H.S., Kerby, T., Calvert, H., 2000. Temozolomide and treatment of malignant glioma. Clin. Cancer Res. 6, 2585–2597.
Frisch, M.J., Trucks, G.W., Schlegel, H.B., Scuseria, G.E., Robb, M.A., Cheeseman, J.R., Scalmani, G., Barone, V., Mennucci, B., Petersson, G.A., Nakatsuji, H., Caricato, M., Li, X., Hratchian, H.P., Izmaylov, A.F., Bloino, J., Zheng, G., Sonnenberg, J.L., Hada, M., Ehara, M., Toyota, K., Fukuda, R., Hasegawa, J., Ishida, M., Nakajima, T., Honda, Y., Kitao, O., Nakai, H., Vreven, T., Montgomery, Jr J.A., Peralta, J.E., Ogliaro, F., Bearpark, M., Heyd, J.J., Brothers, E., Kudin, K. N., Staroverov, V.N., Kobayashi, R., Normand, J., Raghavachari, K., Rendell, A., Burant, J.C., Iyengar, S. S., Tomasi, J., Cossi, M., Rega, N., Millam, N.J., Klene, M., Knox, J.E., Cross, J.B., Bakken, V., Adamo, C., Jaramillo, J., Gomperts, R., Stratmann, R.E., Yazyev, O., Austin, A.J., Cammi, R., Pomelli, C., Ochterski, J.W., Martin, R.L., Morokuma, K., Zakrzewski, V.G., Voth, G.A., Salvador, P., Dannenberg, J.J., Dapprich, S., Daniels, A.D., Farkas, Ö., Foresman, J.B., Ortiz, J.V., Cioslowski, J., Fox, D.J., 2009. Gaussian 09, Revision C.01. Gaussian, Inc., Wallingford.
Happold, C., Roth, P., Wick, W., Schmidt, N., Florea, A.-M., Silginer, M., Reifenberger, G., Weller, M., 2012. Distinct molecular mechanisms of acquired resistance to temozolomide in glioblastoma cells. J. Neurochem. 122, 444–455.
Jensen, F., 2008. Basis set convergence of nuclear magnetic shielding constants calculated by density functional methods. J. Chem. Theor. Comp. 4, 719–727.
Kanugula, S., Pegg, A., 2003. P Alkylation damage repair protein O6-alkylguanine-DNA alkyltransferase from the hyperthermophiles Aquifex aeolicus and Archaeoglobus fulgidus. Biochem J. 375, 449–455.
Łączkowski, K.Z., Anusiak, J., Świtalska, M., Dzitko, K., Cytarska, J., Baranowska-Łączkowska, A., Plech, T., Paneth, A., Wietrzyk, J., Białczyk, J., 2018. Synthesis, molecular docking, ctDNA interaction, DFT calculation and evaluation of antiproliferative and anti-*Toxoplasma gondii* activities of 2,4-diaminotriazine-thiazole derivatives. Med. Chem. Res. 27, 1131–1148.
Łączkowski, K.Z., Misiura, K., Świtalska, M., Wietrzyk, J., Baranowska-Łączkowska, A., Fernández, B., Paneth, A., Plech, T., 2014. Synthesis and *in vitro* antiproliferative activity of thiazole-based nitrogen mustards. The hydrogen bonding interaction between model systems and nucleobases. Anti-Cancer Agents Med. Chem. 14, 1271–1281.
Łączkowski, K.Z., Motylewska, K., Baranowska-Łączkowska, A., Biernasiuk, A., Misiura, K., Malm, A., Fernández, B., 2016. Synthesis, antimicrobial evaluation and theoretical prediction of NMR chemical shifts of thiazole and selenazole derivatives with high antifungal activity against *Candida* spp. J. Mol. Struct. 1108, 427–437.
London, F., 1937. Théorie quantique des courants interatomiques dans les combinaisons aromatiques. J. Phys. Radium 8, 397–409.
Marciniec, K., Bafeltowska, J., Maślankiewicz, M.J., Buszman, E., Boryczka, S., 2016. Determination of the lipophilicity of quinolinesulfonamides by reversed-phase HPLC and theoretical calculations. J. Liq. Chromatogr. Relat. Technol. 39, 702–709.
Marouzi, S., Rad, A.S., Beigoli, S., Baghaee, P.T., Darban, R.A., Chamani, J., 2017. Study on effect of lomefloxacin on human holo-transferrin in the presence of essential and nonessential amino acids: spectroscopic and molecular modeling approaches. Int. J. Biol. Macromol. 97, 688–699.
Mazák, K., Kökösi, J., Noszál, B., 2011. Lipophilicity of zwitterions and related species: a new insight. Eur. J. Pharm. Sci. 44, 68–73.
Meer, L., Janzer, R.C., Kleihues, P., Kolar, G.F., 1986. In vivo metabolism and reaction with DNA of the cytostatic agent, 5-(3,3-dimethyl-1-triazeno)imidazole-4-carboxamide (DTIC). Biochem. Pharmacol. 35, 3243–3247.
Monteiro, A.S., Almeida, J., Cabral, G., Severino, P., Videira, P.A., Sousa, A., Nunes, R., Pereira, J.D., Francisco, A.P., Perry, M.J., Mendes, E., 2013. Synthesis and evaluation of N-acylamino acids derivatives of triazenes. Activation by tyrosinase in human melanoma cell lines. Eur. J. Med. Chem. 70, 1–9.
Moosavi-Movahedi, A.A., Chamani, J., Ghourchian, H., Shafiey, H., Sorenson, C.M., Sheibani, N., 2003. Electrochemical evidence for the molten globule states of cytochrome c induced by N-alkyl sulfates at low concentrations. J. Prot. Chem. 22, 23–30.
Moosavi-Movahedi, A.A., Golchin, A.R., Nazari, K., Chamani, J., Saboury, A.A., Bathaie, S.Z., Tangestani-Nejad, S., 2004. Microcalorimetry, energetics and binding studies of DNA-dimethyltin dichloride complexes. Thermochim. Acta 414, 233–241.
O'Reilly, S.M., Newlands, E.S., Glaser, M.G., Brampton, M., Rice-Edwards, J.M., Illingworth, R.D., 1993. Temozolomide: a new oral cytotoxic chemotherapeutic agent with promising activity against primary brain tumors. Eur. J. Cancer 29, 940–942.
Omidvar, Z., Asoodeh, A., Chamani, J., 2013. Studies on the antagonistic behavior between cyclophosphamide hydrochloride and aspirin with human serum albumin: time-resolved fluorescence spectroscopy and isothermal titration calorimetry. J. Sol. Chem. 42, 1005–1017.
Pakravan, P., Masoudian, S., 2015. Study on the interaction between isatin-β-thiosemicarbazone and calf thymus DNA by spectroscopic techniques. Iran. J. Pharm. Res. 14, 111–123.
Rafique, B., Khalid, A.M., Akhtar, K., Jabbar, A., 2013. Interaction of anticancer drug methotrexate with DNA analyzed by electrochemical and spectroscopic methods. Biosens. Bioelectron. 44, 21–26.
Rashidipour, S., Naeeminejad, S., Chamani, J., 2016. Study of the interaction between DNP and DIDS with human hemoglobin as binary and ternary systems: spectroscopic and molecular modeling investigation. J. Biomol. Struct. Dyn. 34, 57–77.
Rubinstein, L.V., Shoemaker, R.H., Paul, K.D., Simon, R.M., Tosini, S., Skehan, P., Sudiero, D.A., Monks, A., Boyd, M.R., 1990. Comparison of in vitro anticancer-drug-screening data generated with a tetrazolium assay versus a protein assay against a diverse panel of human tumor cell lines. J. Nat. Cancer Inst. 82, 1113–1118.
Schuchardt, K.L., Didier, B.T., Elsethagen, T., Sun, L., Gurumoorthi, V., Chase, J., Li, J., Windus, T.L., 2007. Basis set exchange: a community database for computational sciences. J. Chem. Inf. Model. 47, 1045–1052.
Sidoryk, K., Świtalska, M., Wietrzyk, J., Jaromin, A., Piętka-Ottlik, M., Cmoch, P., Zagrodzka, J., Szczepek, W., Kaczmarek, L., Peczyńska-Czoch, W., 2012. Synthesis and biological evaluation of new amino acid and dipeptide derivatives of neocryptolepine as anticancer agents. J. Med. Chem. 55, 5077–5087.
Smith Jr., R.H., Scudiero, D.A., Michejda, C.J., 1990. 1,3-Dialkyl-3-acyltriazenes, a novel class of antineoplastic alkylating agents. J. Med. Chem. 33, 2579–2583.
Sohrabi, T., Hosseinzadeh, M., Beigoli, S., Saberi, M.R., Chamani, J., 2018. Probing the binding of lomefloxacin to a calf thymus DNA-histone H1 complex by multi-spectroscopic and molecular modeling techniques. J. Mol. Liquids 256, 127–138.
Wietrzyk, J., Chodyński, M., Fitak, H., Wojdat, E., Kutner, A., Opolski, A., 2007. Antitumor properties of diastereomeric and geometric analogs of vitamin D3. Anticancer Drugs 18, 447–457.
Yahalom, J., Voss, R., Leizerowitz, R., Fuks, Z., Polliack, A., 1983. Secondary leukemia following treatment of Hodgkin's disease: ultra structural and cytogenetic data in two cases with a review of the literature. Am. J. Clin. Pathol. 80, 231–236.
Zawilska, J.B., Wojcieszak, J., Olejniczak, A.B., 2013. Prodrugs: a challenge for the drug development. Pharmacol. Rep. 65, 1–14.
Zhang, G., Hu, X., Pan, J., 2011. Spectroscopic studies of the interaction between piricarb and calf thymus DNA. Spectrochim. Acta A Mol. Biomol. Spectrosc. 78, 687–694.